Evolution of breathers with spectrally skewed forcing and damping

Alberto Alberello * and Emilian Părău
School of Engineering, Mathematics and Physics, University of East Anglia, NR4 7TJ Norwich, United Kingdom

(Received 23 May 2025; accepted 3 September 2025; published 1 October 2025)

Slowly modulated nonlinear waves are accurately described in the framework of the conservative nonlinear Schrödinger equation (NLS). However, in many physical systems, the wave evolution is affected by energy gains and losses, therefore requiring introduction of forcing or damping in the NLS framework. Here, we analyze the idealized case in which the forcing term varies linearly with frequency such as the growth rate of positive components matches the decay rate of the negative ones. We reveal that the system is linearly unstable and prone to overall energy growth. The evolution of classical breather solutions is showcased in this framework. The most notable effects are the distortion of the breathers, which speed-up, and in the case of the Kuznetsov-Ma breather results in faster recurrence. Concurrently, spectral asymmetry between low and high frequency components develops.

DOI: 10.1103/7ykg-j215

I. INTRODUCTION

The nonlinear Schrödinger equation (NLS) is widely used across numerous physical systems to model the dynamics of the slow modulation of weakly nonlinear, dispersive, wave packets [1]. Applications of the NLS span optics [2–5], quantum dynamics [6–8], ocean dynamics [9,10], and metamaterials [11]. Within the NLS framework, breather solutions, which are periodic solutions in time or space and localized in space and/or time, have been thoroughly studied [12–15]. Unlike solitonic solutions that emerge from a zero background at infinity, breathers emerge from perturbation of the uniform, nonzero, background and are an archetype for weakly nonlinear dispersive wave packets as they are observed nature.

External forcing (positive and/or negative) affects the wave dynamics in many real-world physical systems. For example, in the context of ocean waves, loss is associated to viscous-like attenuation at the interface [16–18] and gain to wind input [19,20]. Such effects have been introduced in the NLS framework by including a homogeneous forcing (or damping), also in the context of the higher-order NLS [21–23]. Forcing (and damping) is a linear operator [24] which leads to net energy gain or loss depending on the sign of the forcing [19,20]. Within this context, Onorato and Proment [20] found approximate rogue wave solutions of classical breather solutions (Peregrine [14], Kuznetsov-Ma [12,13], and Akhmediev [15,25]) and, as also shown in Segur *et al.* [17] and Kharif *et al.* [19], found that forcing (damping) destabilizes (stabilizes) modulational instability.

However, forcing can be heterogeneous (e.g., frequency-dependent) as in the case of waves in sea ice [26–30], optical cavities [4], nonlinear optics [31], Bose-Einstein condensates [3], plasma [7], and metamaterials [11]. Humphries *et al.* [23] considered the case of heterogeneous loss counterbalanced by homogeneous gain such as the system energy is conserved and focused on the evolution of solitonic solutions. Even in a conservative system, the net imbalance between high and low frequencies was found to generate a richer dynamics.

Here, we build on the theoretical work of Slunyaev and Stepanyants [30] in which the heterogeneous forcing in the NLS was derived rigorously by expansion of the frequency-dependent term, therefore, obtaining a homogeneous (constant) forcing plus an heterogeneous part which varies linearly with frequency. Similarly to Eeltink *et al.* [22], in this study we suppress the homogeneous forcing, but, unlike them, in our system the decay rate of high frequency is balanced by an equal but opposite growth rate of low frequencies at the leading order (and not at higher order). It is in this framework, that is fundamentally different from the one of Onorato and Proment [20] in which forcing was assumed to be homogeneous, that we analyze the evolution of archetypical breather solutions (Peregrine, Kuznetsov-Ma, and Akhmediev).

II. FORMULATION

In dimensionless form, the NLS with (negative) forcing reads

$$i\psi_\chi + \psi_{\tau\tau} + 2|\psi|^2\psi = -i\mathcal{D}\psi, \tag{1}$$

where $\mathcal{D} > 0$ is the dimensionless attenuation rate along χ. In the case of frequency-dependent damping $\mathcal{D}$ is a function of frequency detuning [$\mathcal{D}(\omega)$; higher frequencies are subjected to stronger attenuation–note that ω is the spectral variable for τ], of the type $\mathcal{D}_0\omega^n$ [28] where $\mathcal{D}_0$ and n are constants and depend on the specific physical process.

The forcing $\mathcal{D}(\omega)$, following Slunyaev and Stepanyants [30], can be replaced by the first two terms of its Taylor series. Moreover, using the correspondence between the dispersion

*Contact author: a.alberello@uea.ac.uk

relation and linear partial differential equation ($\omega \to i\,\partial/\partial\tau$) it can be rewritten as

$$i\psi_\chi + \psi_{\tau\tau} + 2|\psi|^2\psi = -i\mathcal{D}_0\psi + n\mathcal{D}_0\psi_\tau. \tag{2}$$

Note that this equation [Eq. (2)] matches the formulation of Slunyaev and Stepanyants [30] (the transformation in dimensional form for the water waves problem is presented in Appendix).

Since we are interested in only the heterogeneous part, we suppress the homogeneous (frequency-independent) part of the forcing ($-i\mathcal{D}_0\psi$; in practice this is achieved by imposing a forcing of opposite sign). A similar assumption was made in Eeltink *et al.* [22] for their leading-order term. Within this framework, the carrier frequency ($\omega = 0$) is subjected to neither forcing nor damping.

Without loss of generality, we consider $n = 1$ which corresponds to a linearly varying forcing with the frequency (positive for negative frequencies and negative for positive frequencies assuming $\mathcal{D}_0 > 0$). The resulting equation is

$$i\psi_\chi + \psi_{\tau\tau} + 2|\psi|^2\psi = \mathcal{D}_0\psi_\tau. \tag{3}$$

It is worth nothing that the right-hand side (RHS) in Eq. (3) resembles the higher-order forcing and damping in Eeltink *et al.* [22]. However, the most striking difference is that in their framework this term (the τ derivative for forcing and damping) only appears at higher order in wave steepness to match their higher-order NLS whereas in our framework it already appears at order $\mathcal{O}(1)$. Therefore, in Eeltink *et al.* [22] the differential growth and decay of frequency components across the spectrum (and the ensuing spectral asymmetry and down- or up-shift) is a higher-order effect, but in our framework, and similarly in Slunyaev and Stepanyants [30] and Humphries *et al.* [23], it is a leading-order effect.

While the stability or instability of the NLS equation under homogeneous damping ajd forcing has been extensively studied [17–19], it is instructive to retrieve the dispersion relation of the proposed model, i.e., Eq. (3), that reads

$$k(\omega) = \omega^2 + \mathcal{D}_0 i\omega - 2|\psi|^2, \tag{4}$$

and linearizing

$$k(\omega) = \omega^2 + \mathcal{D}_0 i\omega \tag{5}$$

in which we note that an imaginary part is, in general, always present as expected for a nonconservative system and indicates growth (assuming $\mathcal{D}_0 > 0$).

III. NUMERICAL EXPERIMENTS

Classical breather solutions are given by rational solutions of the NLS, nominally the Peregrine, Akhmediev, and Kuznetsov-Ma breathers [20,32]. The Akhmediev breather describes the full growth-return cycle that starts with modulation instability at $\chi \to -\infty$, where the solution corresponds to the plane wave [32], reaches maximum amplification for $\chi = 0$, and returns to a plane wave solution at $\chi \to +\infty$. The Akhmediev breather is periodic in τ, the Kuznetsov-Ma breather is localized in τ and periodic in χ. The Peregrine breather, which can be seen as an extreme Akhmediev and Kuznetsov-Ma when periodicity tends to infinity, is doubly localized in time and space.

The Peregrine, Akhmediev, and Kuznetsov-Ma breather solutions are

$$\psi_P = \left[\frac{4(1+4i\chi)}{1+4\tau^2+16\chi^2} - 1\right]\exp(2i\chi), \tag{6}$$

$$\psi_A = \left[\frac{\nu^3\cosh(\sigma\chi) + i\nu\sigma\sinh(\sigma\chi)}{2\nu\cosh(\sigma\chi) - \sigma\cos(\nu\tau)} - 1\right]\exp(2i\chi), \tag{7}$$

$$\psi_{\mathrm{KM}} = \left[\frac{\mu^3\cos(\rho\chi) + i\mu\rho\sin(\rho\chi)}{2\mu\cos(\rho\chi) - \rho\cosh(\mu\tau)} + 1\right]\exp(2i\chi), \tag{8}$$

where $\sigma = \nu\sqrt{4-\nu^2}$ (with $0 < \nu < 2$) and $\rho = \mu\sqrt{4+\mu^2}$ (with $\mu > 0$). The maximum amplification for the Peregrine breather is 3, for the Akhmediev breather $AF_A = 1 + \sqrt{4-\nu^2}$, and for the Kuznetsov-Ma $AF_{\mathrm{KM}} = 1 + \sqrt{4+\mu^2}$. It is worth noting that $AF_P = \lim_{\mu\to 0} AF_{\mathrm{KM}}(\mu) = \lim_{\nu\to 0} AF_A(\nu)$ (see [33]).

We perform numerical simulations of the breather solutions. Given $\psi_0 = \psi(\chi = \chi_0)$, obtained from the analytical breather solution [Eqs. (6)–(8)], the evolution $\psi(\chi)$ can be effectively simulated with the split-step method

$$\psi(\chi + d\chi) = \mathcal{F}^{-1}\{e^{[-2\mathcal{D}_0\omega - i\omega^2]d\chi}\mathcal{F}[e^{2i|\psi|^2 d\chi}\psi(\chi)]\} \tag{9}$$

in which $\mathcal{F}$ and $\mathcal{F}^{-1}$ denote the Fourier transform and its inverse, i.e., $\mathcal{F}\{\psi(\chi,\tau)\} = \hat{\psi}(\chi,\omega)$. Note that in this numerical implementation the forcing term is part of the linear operator and therefore efficiently computed in Fourier space. Numerical simulations will be performed over $-\pi/2 \leqslant \chi \leqslant +\pi/2$ (discretized with 1536 elements) and $-16\pi \leqslant \tau \leqslant 16\pi$ (discretized with 1024 elements). The wide domain in τ is chosen to avoid side effects, and the analysis will only focus on the central portion of the domain.

We will showcase the effect of varying $\mathcal{D}_0 \in [0, 6\times 10^{-3}, 12\times 10^{-3}]$ to span a range of configurations maintaining the parameter $\mathcal{D}_0$ small. A higher value of the parameter $\mathcal{D}_0$ would lead to an explosion of the numerical solution because, while some spectral components are damped others are forced, leading to an overall growth as previously observed in [22] and Humphries *et al.* [23]. It is also worth noting that for negative values of $\mathcal{D}_0$ the same solution is obtained by applying the transformation $\tau \to -\tau$ (and $\omega \to -\omega$). Moreover, we arbitrarily set $\nu = 1$ for the Akhmediev breather, which yields $AF_A = 1 + \sqrt{3} \approx 2.73$, and $\mu = 2$ for the Kuznetsov-Ma breather, which yields $AF_{\mathrm{KM}} = 1 + 2\sqrt{2} \approx 3.83$.

In the following, we will report the numerical results in the physical and spectral domain. Invariants of the conservative NLS, wave action $\mathcal{N}$, and momentum $\mathcal{M}$ will be monitored:

$$\mathcal{N} = \int_{-\infty}^{+\infty} |\psi|^2 d\tau, \tag{10}$$

$$\mathcal{M} = \frac{1}{2i}\int_{-\infty}^{+\infty} (\psi\psi_\tau^* - \psi^*\psi_\tau) d\tau, \tag{11}$$

where ψ^* denotes the complex conjugate of ψ.

We also introduce the spectral asymmetry A:

$$A(\chi) = \frac{\int_{-\infty}^{0^-} |\hat{\psi}| d\omega - \int_{0^+}^{+\infty} |\hat{\psi}| d\omega}{\int_{-\infty}^{+\infty} |\hat{\psi}(\chi = \chi_0)| d\omega}. \tag{12}$$

This quantity measures the energy imbalance between the two halves of the spectrum.

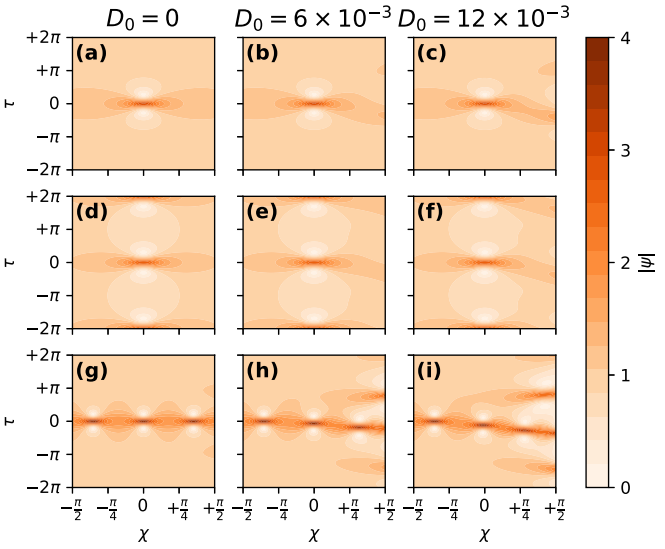

FIG. 1. Breather solutions from top to bottom Peregrine, Akhmediev, Kuznetsov-Ma with various level of $\mathcal{D}_0$ from left to right $0, 6 \times 10^{-3}, 12 \times 10^{-3}$.

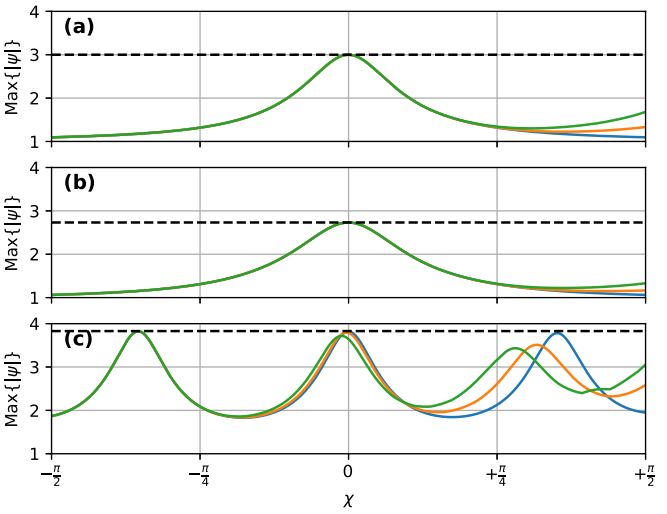

FIG. 2. Maximum amplitude of the breather solutions from top to bottom Peregrine, Akhmediev, Kuznetsov-Ma with various levels of $\mathcal{D}_0$ (blue $\mathcal{D}_0 = 0$; orange $\mathcal{D}_0 = 6 \times 10^{-3}$; green $\mathcal{D}_0 = 12 \times 10^{-3}$). The black dashed line denotes the maximum amplification.

IV. RESULTS

The breather solution in the physical space (χ, τ) is shown in Fig. 1. When $\mathcal{D}_0 = 0$, i.e., there is no forcing, as expected, the evolution corresponds to theoretical expectations for the Peregrine and Akhmediev, but, for the chosen numerical implementation, the Kuznetsov-Ma slightly deviates from prediction after the first focusing cycle in our numerics. Nevertheless, the difference between numerical simulations from the theoretical predictions are small, and we therefore choose to proceed with these numerical parameters (we will later show the wave action, and that is conserved providing confidence in the numerical results).

When $\mathcal{D}_0 \neq 0$ (second and third columns in Fig. 1) the most striking difference is the tilting of the breather towards negative τ which corresponds to a speed-up of the solution for $\mathcal{D}_0 > 0$. This is the expected outcome for dispersive waves when shorter, slower, components are attenuated while the longer, faster, components gain energy. In the case of the Kuznetsov-Ma breather is also evident a shortening of the recurrence. The shortening was also noted by Onorato and Proment [20] for homogeneous forcing, but, unlike in our simulations, no speed-up (or slow-down) was observed. The other notable feature in our simulations for the Peregrine and Akhmediev breathers is the emergence of a second growth cycle.

The recurrency of the breather solution appears more clearly visible in profiles of the solution as shown in Fig. 2(c) (note that the profiles are extracted at the $\max_\tau |\psi(\chi)|$ rather than at a constant τ to better capture the shape of the drifting breathers), where it is also apparent that at subsequent recurrence cycles the maximum amplification gets reduced, as observed in Alberello *et al.* [28] but for dissipation only.

The observed behavior is qualitatively similar to the one shown by Eeltink *et al.* [22], however, the key difference is that in their model the behavior is associated with higher-order terms in the NLS whereas in ours it is a leading-order effect driven by the spectrally skewed forcing and damping. It could be argued that in many physical settings it would be preferable to use a simpler model, like in our approach, with a more physically based and true-to-reality choice of the forcing and damping rather than invoking higher-order nonlinearity.

The depiction of the Fourier spectrum (Fig. 3) confirms the observation made in the physical space. It should be noted that while the Peregrine and Kuznetsov-Ma breathers form a pseudocontinuous Fourier spectrum (because a discrete Fourier transform is applied, strictly speaking, the spectrum is discrete), the Akhmediev breather shows a discrete spectrum in Fourier space. It is nevertheless instructive to analyze the asymmetry of the spectrum (Fig. 4). In these the asymmetry between positive and negative frequencies when $\mathcal{D}_0 \neq 0$ is apparent, which is similar for the Peregrine and Akhmediev

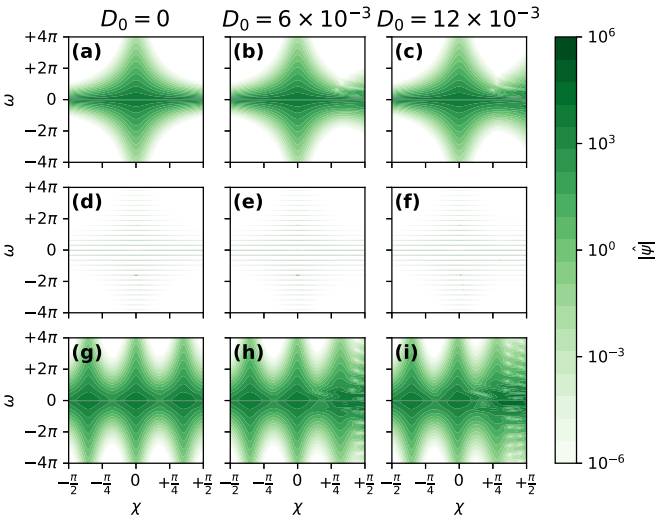

FIG. 3. Spectra of breather solutions from top to bottom Peregrine, Akhmediev, Kuznetsov-Ma with various levels of $\mathcal{D}_0$ from left to right $0, 6 \times 10^{-3}, 12 \times 10^{-3}$.

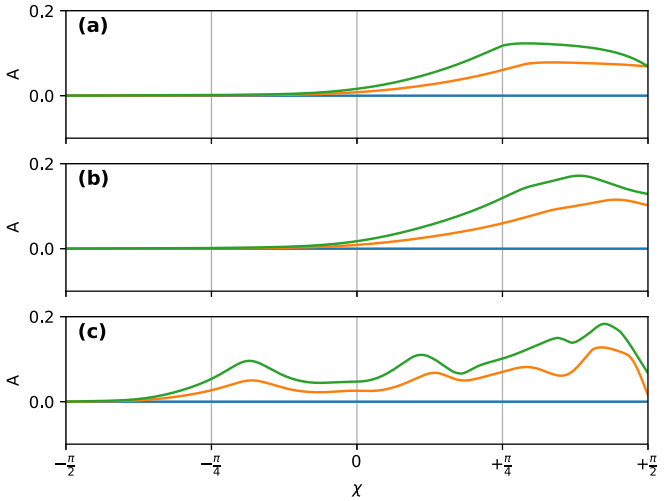

FIG. 4. Spectral asymmetry of the breather solutions from top to bottom Peregrine, Akhmediev, Kuznetsov-Ma with various levels of $\mathcal{D}_0$ (colors as in Fig. 2).

breathers and clearly increases just before the maximum amplification. As expected, positive frequencies have a lower energy content from their negative counterpart. The differences are more notable when $\mathcal{D}_0$ increases. The asymmetry emerging for $\mathcal{D}_0 > 0$ will lead to a downshift of the spectrum over longer distance. More complex interactions appear to be in place for the Kuznetsov-Ma breather for which the asymmetry undergoes growth and decay cycles while staying positive.

Finally, it is instructive to analyze some of the conserved quantities in the classical NLS: the wave action and momentum. These are shown in Fig. 5 where the first column actually shows the relative variation, i.e., $\Delta\mathcal{N} = \mathcal{N}(\chi)/\mathcal{N}(\chi_0) - 1$. As expected, for the conservative case ($\mathcal{D}_0 = 0$) wave action is preserved, but when $\mathcal{D}_0 > 0$ there is an increase of

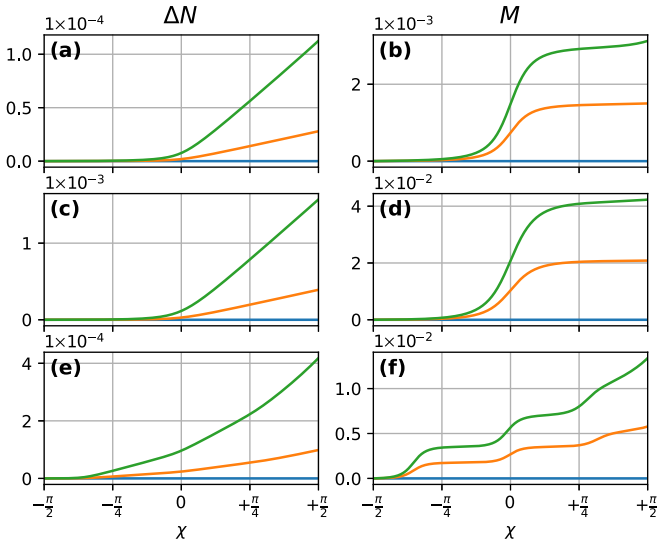

FIG. 5. Relative change in wave action (left) and momentum (right) of the breather solution from top to bottom Peregrine, Akhmediev, Kuznetsov-Ma with various levels of $\mathcal{D}_0$ (colors as in Fig. 2).

wave action. To a certain extent this should be expected because even in the linear regime a energy mismatch between left and right sidebands emerges, i.e., the energy gained on one side exceeds the loss on the other. To better demonstrate the increase in wave action, we consider two components at $-\omega$ and $+\omega$, respectively. For these two components, due to the symmetry of the initial spectrum, the initial energy is $\mathcal{N}_0^{\pm\omega} = (a^+)^2 + (a^-)^2 = 2a_0^2$ where $a_0 = |\hat{\psi}_0(\pm\omega)|$ and the superscript denotes the components at $\pm\omega$. In the linear system, applying the growth rate, we obtain $a^{\pm}(\chi) = a_0 \exp(\pm\mathcal{D}_0\omega\chi)$. The corresponding wave action is $\mathcal{N}^{\pm\omega}(\chi) = a_0^2[\exp(-\mathcal{D}_0\omega\chi)^2 + \exp(+\mathcal{D}_0\omega\chi)^2] = a_0^2\, 2\cosh(2\mathcal{D}\omega_0\chi) \geqslant 2|a_0|^2$ since $\cosh x > 1$ for every $x \neq 0$, therefore, explaining why an increase in wave action along χ is expected. Nevertheless, it is worth noting that the change in wave action is amplified in the nonlinear regime, and is between one and two orders of magnitude greater than in the linear system. The wave action increase is more limited in the Peregrine breather, while it is almost one order of magnitude greater for the Akhmediev and Kuznetsov-Ma solutions (the Akhmeniedev breather approximately double the Kuznetsov-Ma breather). Notably, the growth rate in wave action seems to increase at every focusing (see in particular the Kuznetsov-Ma). The momentum, increases when $\mathcal{D}_0 > 0$. This is also true in the linear regime where momentum increases linearly. However, in the nonlinear regime, there is a sharp increase at each focusing cycle, i.e., when the amplitude of the envelope peaks, and the change is two orders of magnitude greater than in linear simulations. The variation is similar in magnitude for the Akhmediev and Kuznetsov-Ma solutions and much smaller for the Peregrine breather.

V. SUMMARY

We introduced a NLS model with heterogeneous, spectrally skewed, forcing in which the zero mode is subjected to neither forcing nor damping. While highly idealized, the model has the potential to replicate real-world physical systems. One of the most remarkable results is that the model qualitatively replicates features obtained with more complex models, i.e., the higher-order NLS of Eeltink *et al.* [22], without the need of including these complexities. Therefore, we believe that in many applications it would be preferable to employ a simple model, like the one that we use, and adopt a more physically inspired choice of forcing.

ACKNOWLEDGMENTS

This work was stimulated by discussions during the "*Maths of Sea Ice*" (Ref. EP/V521929/1) meeting which was made possible by the Isaac Newton Institute for Mathematical Sciences. We acknowledge funding from Royal Society (IECR3243016). The authors thank Dr. A. Villois and Dr. B. S. Humphries for fruitful discussions.

DATA AVAILABILITY

The data that support the findings of this article are not publicly available. The data are available from the authors upon reasonable request.

APPENDIX: TRANSFORMATION FOR THE WATER WAVES PROBLEM

Equations (2) and (3) are written in dimensionless form. For spatial evolution of a wave train in the frame of reference moving with the group velocity, as needed to better replicate experimental observations, the following transformations applies:

$$\mathcal{D}_0 = \frac{g}{2\omega_0} D_0; \tag{A1}$$

$$\tau = \frac{2\omega_0}{g} t; \tag{A2}$$

$$\chi = \frac{4\omega_0^2}{g} x; \tag{A3}$$

$$\psi = \frac{\omega_0^2}{2g\sqrt{2}} u; \tag{A4}$$

where ω_0 is the angular frequency of the carrier wave, g gravity, x and t are the spatial and temporal coordinates, u the envelope amplitude, and D_0 the forcing parameter. Note that the transformation matches the one presented in Slunyaev and Stepanyants [30] when inertia is absent. The surface elevation η is obtained from the wave envelope

$$\eta(x,t) = \mathrm{Re}\{u(x,t)e^{i[k(\omega_0)x-\omega_0 t]}\}. \tag{A5}$$

A note should be added in regard to the value D_0 in dimensional form. The value corresponds to small attenuation with reference to Alberello *et al.* [28], and is significantly lower than the one observed in many real-world scenarios for ocean waves. However, while the absolute value is low, the relative variation across frequency reflects the one encountered in many physical problems.

[1] M. Onorato, S. Residori, U. Bortolozzo, A. Montina, and F. Arecchi, Rogue waves and their generating mechanisms in different physical contexts, Phys. Rep. **528**, 47 (2013).

[2] M. Nagasawa, *Schrödinger Equations and Diffusion Theory* (Springer Science & Business Media, New York, 1993).

[3] H. Deng, H. Haug, and Y. Yamamoto, Exciton-polariton Bose-Einstein condensation, Rev. Mod. Phys. **82**, 1489 (2010).

[4] T. Herr, V. Brasch, J. D. Jost, C. Y. Wang, N. M. Kondratiev, M. L. Gorodetsky, and T. J. Kippenberg, Temporal solitons in optical microresonators, Nat. Photon. **8**, 145 (2014).

[5] U. Younas, T. A. Sulaiman, and J. Ren, On the study of optical soliton solutions to the three-component coupled nonlinear Schrödinger equation: Applications in fiber optics, Opt. Quantum Electron. **55**, 72 (2023).

[6] H. Conroy, Molecular Schrödinger equation. VIII. A new method for the evaluation of multidimensional integrals, J. Chem. Phys. **47**, 5307 (1967).

[7] P. K. Shukla and B. Eliasson, Nonlinear aspects of quantum plasma physics, Phys. Usp. **53**, 51 (2010).

[8] G. El and A. Tovbis, Spectral theory of soliton and breather gases for the focusing nonlinear Schrödinger equation, Phys. Rev. E **101**, 052207 (2020).

[9] C. Sulem and P.-L. Sulem, *The Nonlinear Schrödinger Equation: Self-Focusing and Wave Collapse* (Springer Science & Business Media, New York, 1999), Vol. 139.

[10] F. Copie, S. Randoux, and P. Suret, The physics of the one-dimensional nonlinear Schrödinger equation in fiber optics: Rogue waves, modulation instability and self-focusing phenomena, Rev. Phys. **5**, 100037 (2020).

[11] A. Demiquel, V. Achilleos, G. Theocharis, and V. Tournat, Modulation instability in nonlinear flexible mechanical metamaterials, Phys. Rev. E **107**, 054212 (2023).

[12] Y.-C. Ma, The perturbed plane-wave solutions of the cubic Schrödinger equation, Stud. Appl. Math. **60**, 43 (1979).

[13] E. A. Kuznetsov, Solitons in a parametrically unstable plasma, Akad. Nauk SSSR Dokl. **236**, 575 (1977) [Sov. Phys. Dokl. **22**, 507 (1977)].

[14] D. H. Peregrine, Water waves, nonlinear Schrödinger equations and their solutions, J. Aust. Math. Soc. Series B, Appl. math. **25**, 16 (1983).

[15] N. N. Akhmediev, V. M. Eleonskii, and N. Kulagin, Exact first-order solutions of the nonlinear Schrödinger equation, Theor. Math. Phys. **72**, 809 (1987).

[16] F. Dias, A. Dyachenko, and V. Zakharov, Theory of weakly damped free-surface flows: A new formulation based on potential flow solutions, Phys. Lett. A **372**, 1297 (2008).

[17] H. Segur, D. Henderson, J. Carter, J. Hammack, C.-M. Li, D. Pheiff, and K. Socha, Stabilizing the Benjamin–Feir instability, J. Fluid Mech. **539**, 229 (2005).

[18] G. Wu, Y. Liu, and D. K. P. Yue, A note on stabilizing the Benjamin–Feir instability, J. Fluid Mech. **556**, 45 (2006).

[19] C. Kharif, R. A. Kraenkel, M. A. Manna, and R. Thomas, The modulational instability in deep water under the action of wind and dissipation, J. Fluid Mech. **664**, 138 (2010).

[20] M. Onorato and D. Proment, Approximate rogue wave solutions of the forced and damped nonlinear Schrödinger equation for water waves, Phys. Lett. A **376**, 3057 (2012).

[21] A. Armaroli, D. Eeltink, M. Brunetti, and J. Kasparian, Nonlinear stage of Benjamin-Feir instability in forced/damped deep-water waves, Phys. Fluids **30**, 017102 (2018).

[22] D. Eeltink, A. Lemoine, H. Branger, O. Kimmoun, C. Kharif, J. D. Carter, A. Chabchoub, M. Brunetti, and J. Kasparian, Spectral up- and downshifting of Akhmediev breathers under wind forcing, Phys. Fluids **29**, 107103 (2017).

[23] B. S. Humphries, J. S. Keeler, A. Alberello, and E. I. Părău, Evolution of nonlinear waves with heterogeneous damping and forcing, Wave Motion **134**, 103482 (2025).

[24] J. S. Keeler, B. S. Humphries, A. Alberello, and E. Părău, Parameter-free higher-order Schrödinger systems with weak dissipation and forcing, Proc. R. Soc. A. **481**, 20240967 (2025).

[25] N. N. Akhmediev, A. Ankiewicz *et al.*, *Nonlinear Pulses and Beams* (Springer, New York, 1997).

[26] A. Alberello and E. Părău, A dissipative nonlinear Schrödinger model for wave propagation in the marginal ice zone, Phys. Fluids **34**, 061702 (2022).

[27] A. V. Slunyaev and Y. A. Stepanyants, Modulation property of flexural-gravity waves on a water surface covered by a compressed ice sheet, Phys. Fluids **34**, 077121 (2022).

[28] A. Alberello, E. Părău, and A. Chabchoub, The dynamics of unstable waves in sea ice, Sci. Rep. **13**, 13654 (2023).

[29] R. Stuhlmeier, C. Heffernan, A. Alberello, and E. Părău, Modulational instability of nonuniformly damped, broad-banded waves: Applications to waves in sea ice, Phys. Rev. Fluids **9**, 094802 (2024).

[30] A. V. Slunyaev and Y. A. Stepanyants, Frequency downshifting in decaying wavetrains on the ocean surface covered by ice floes, Phys. Fluids **36**, 036621 (2024).

[31] C. Naveau, P. Szriftgiser, A. Kudlinski, M. Conforti, S. Trillo, and A. Mussot, Experimental characterization of recurrences and separatrix crossing in modulational instability, Opt. Lett. **44**, 5426 (2019).

[32] A. Chabchoub, B. Kibler, J. M. Dudley, and N. Akhmediev, Hydrodynamics of periodic breathers, Philos. Trans. R. Soc. A **372**, 20140005 (2014).

[33] N. Karjanto, Peregrine soliton as a limiting behavior of the Kuznetsov-Ma and Akhmediev breathers, Front. Phys. **9**, 599767 (2021).